HHS Public Access

Author manuscript

ACS Sens. Author manuscript; available in PMC 2020 May 24.

Published in final edited form as:

ACS Sens. 2019 May 24; 4(5): 1391–1398. doi:10.1021/acssensors.9b00360.

Kinetics-Based Measurement of Hypoxia in Living Cells and Animals Using an Acetoxymethyl Ester Chemiluminescent Probe

Lucas S. Ryan[†], **Jeni Gerberich**[‖], **Jian Cao**[†,⊥], **Weiwei An**[†], **Becky A. Jenkins**[†], **Ralph P. Mason**[‖], and **Alexander R Lippert**[*,†,‡,§]

[†]Department of Chemistry, Southern Methodist University, Dallas, Texas 75275-0314, United States

[‡]Center for Drug Discovery, Design, and Delivery (CD4), Southern Methodist University, Dallas, Texas 75275-0314, United States

[§]Center for Global Health Impact (CGHI), Southern Methodist University, Dallas, Texas 75275-0314, United States

[‖]Prognostic Imaging Research Laboratory (PIRL), Pre-clinical Imaging Section, Department of Radiology, UT Southwestern Medical Center, Dallas, Texas 75390-9058, United States

Abstract

Oxygenation and tissue hypoxia play critical roles in mammalian biology and contribute to aggressive phenotypes in cancerous tumors, driving research to develop accurate and easy-to-implement methods for monitoring hypoxia in living cells and animal models. This study reports the chemiluminescent probe HyCL-4-AM, which contains a nitroaromatic sensing moiety and, importantly, an acetoxymethyl (AM) ester that dramatically improves operation in cells and animals. HyCL-4-AM provides a selective 60 000-fold increase in luminescence emission in the presence of rat liver microsomes (RLM). For cellular operation, the chemiluminescence response kinetics is sharply dependent on oxygen levels, enabling highly significant and reproducible measurement of hypoxia in living cells. Whole animal imaging experiments in muscle tissue and tumor xenografts show that HyCL-4-AM can differentiate between well oxygenated muscle tissue and hypoxic tumors, demonstrating potential for monitoring tumor reoxygenation via hyperoxic treatment.

Graphical Abstract

[*]**Corresponding Author** alippert@smu.edu. Fax: 214-768-4089.

[⊥]J.C.: Department of Biological Chemistry, University of California, Los Angeles, CA 90095.

Author Contributions

The manuscript was written through contributions of all authors. All authors have given approval to the final version of the manuscript.

Supporting Information

The Supporting Information is available free of charge on the ACS Publications website at DOI: 10.1021/acssensors.9b00360.

Synthetic procedures, absorption and emission spectra, detailed procedures for selectivity tests, supplementary procedures and figures, and scanned spectra (PDF)

The authors declare the following competing financial interest(s): A.R.L. discloses a financial stake in BioLum Sciences, LLC, a company developing technology for home-monitoring of asthma.

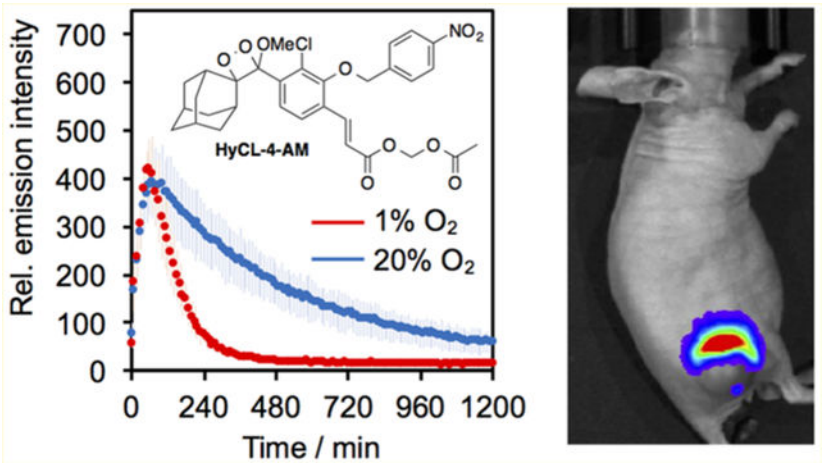

Keywords

chemiluminescence; hypoxia; 1,2-dioxetanes; nitroreductase; in vivo imaging

Oxygen provides a critical energy source for aerobic organisms, necessitating sophisticated cellular machinery to sense and respond to fluxes in oxygen concentration.[1] Hypoxia, a state of low tissue oxygenation, is a physiological outcome of tumors outgrowing their own blood supply. Hypoxic tissues undergo a series of changes mediated by reduced O_2-dependent activity of a prolyl hydroxylase domain (PHD) enzyme that results in activation and heterodimerization of the transcription factors hypoxia inducible factor 1α (HIF-1α) and HIF-1β.[1] This heterodimer promotes the expression of a multitude of downstream targets that promote angiogenesis,[2] growth,[3] and metastasis,[4] while suppressing natural and drug-induced apoptosis.[5,6] Hypoxia shows promise as a prognostic indicator and has been correlated with, for example, poor outcomes in patients with nonsmall cell lung cancer[7] and reduced response to radiotherapy in patients with cervical cancer.[8] The fundamental importance of tissue oxygenation in cancer and other physiological and pathological conditions drives our efforts to develop sensitive and specific measurement methods for the clinic and preclinical laboratory settings.[9]

Methods for clinical hypoxia detection in patients include oxygen electrodes,[7] blood oxygen and tissue oxygen level dependent magnetic resonance imaging (BOLD and TOLD),[10,11] and positron emission tomography/computed tomography (PET/CT).[8] These methods show excellent clinical promise, but either are invasive in the case of electrodes or require expensive instrumentation and expertise in the case of MRI and PET. These obstacles have caused preclinical laboratory efforts to gravitate toward less expensive and easier to implement optical methods for hypoxia imaging.[12] Many optical, as well as PET and immunohistochemical, approaches rely on the selective reduction of nitroaromatic compounds under hypoxic conditions.[13–16] The first step in this reduction process forms the nitroaromatic radical anion ($RNO_2^{-\bullet}$) and can be mediated by a range of enzymes including cytochrome P450 reductase,[17] cytochrome *c* reductase,[18] xanthine oxidase,[19] and lipoamide dehydrogenase.[20] Molecular oxygen, however, can reverse this step by reoxidizing the radical anion with concomitant formation of superoxide. In the absence of O_2, the reduction

can proceed beyond $RNO_2^{-\bullet}$ to the subsequent nitroso, hydroxylamine, and amine compounds. This mechanism has been exploited to develop sensitizers for radiation and chemotherapy, as well as compounds to aid in hypoxia imaging and detection.[21] Fluorescent,[12] photoacoustic,[22] bioluminescent,[23] and chemiluminescent[24,25] imaging agents based on this approach have been reported. While many strides have been made in fluorescence technology for hypoxia imaging, chemiluminescence offers a distinct advantage by directly generating light from the energy of a chemical bond without requiring an external light source or genetic modifications.[26] This simplifies experiments and inherently increases sensitivity and tissue imaging depth by drastically attenuating autofluorescence and light scattering effects.[27,28] Indeed, recent advances in triggered spiroadamantane 1,2-dioxetane chemiluminescence technology have allowed for high quantum yields in aqueous systems,[29–31] and have been applied for the detection of peroxynitrite,[32] nitroxyl,[33] formaldehyde,[34] prodrug release,[35] cathepsin B,[36] NQO1,[37] transition metals,[38] and other analytes.[27]

Here, we use enzymatic reduction of a nitroaromatic moiety to trigger light emission for the development of Hypoxia ChemiLuminescence probe 3 (HyCL-3) and HyCL-4-AM (Scheme l). While previously reported HyCL-2[24] and CL-NTR[25] were demonstrated to be responsive to tissue oxygenation in vitro and in animal experiments, none of these probes were successfully employed in cells and only limited data was acquired for animal imaging. In this study, we evaluate HyCL-3 and HyCL-4-AM as chemiluminescent reporters for hypoxia in vitro, in cellulo, and in vivo. Importantly, we demonstrate that incorporation of an acetoxymethyl (AM) ester dramatically improves operation in cellular systems and increases the response in whole animal tumor xenograft models versus previously disclosed chemiluminescent probes.

EXPERIMENTAL SECTION

General Synthetic Methods.

All reactions were performed in dried glassware under an atmosphere of dry N_2. Reagents were purchased from Sigma-Aldrich (St. Louis, MO), Alfa Aesar (Ward Hill, MA), EMD Millipore (Billerica, MA), Oakwood Chemical (West Columbia, SC), and Cayman Chemical (Ann Arbor, MI) and used without further purification. ^{1}H NMR and ^{13}C NMR spectra for characterization of new compounds and monitoring reactions were collected in $CDCl_3$ (Cambridge Isotope Laboratories, Cambridge, MA) on a JEOL 500 MHz spectrometer or a Bruker 400 MHz spectrometer in the Department of Chemistry at Southern Methodist University. All chemical shifts are reported in the standard notation of parts per million using the peak of residual proton signals of the deuterated solvent as an internal reference. High resolution mass spectroscopy was performed on a Shimadzu IT-TOF (ESI source) at the Shimadzu Center for Advanced Analytical Chemistry at the University of Texas, Arlington and low resolution mass spectroscopy was performed on an Advion CMS (ESI source) at Southern Methodist University. Detailed synthetic procedures can be found in the Supporting Information.

Chemiluminescence Response of HyCL-3 and HyCL-4-AM to NTR and NADH and Rat Liver Microsomes (RLM).

Chemiluminescent emission wavelength spectra were acquired using a Hitachi F-7000 fluorescence spectrophotometer via the luminescence detection module and scanning luminescence emission from 400–700 nm in response to NTR and NADH. Final concentrations of 200 μM NADH, 1 μg mL^{-1} nitroreductase from *Escherichia coli* (NTR, Sigma-Aldrich N9284–1MG) in DI-H_2O, and 10 μM HyCL-3 or HyCL-4-AM were added to a solution of 20 mM PBS buffered to pH 7.41. A final concentration of 1 U mL^{-1} pig liver esterase (PLE) was also added for HyCL-4-AM reads. Scans were acquired using the wavelength scan module 10 min after addition of the probe to the solution. Dose dependent responses to NTR and NADH for HyCL-3 and HyCL-4-AM from 0 to 1000 ng mL^{-1} NTR were acquired using a Cytation 5 BioTek plate reader via the luminescence detection mode, end point read type. The temperature was set at 37 °C under ambient atmosphere. The gain was set at 135 and the read height was set at 4.5 mm. In a 96-well plate, 10 μM HyCL-3 or HyCL-4-AM in 20 mM PBS buffered to pH 7.4, containing ≤1% DMSO, were treated 0–1000 ng mL^{-1} NTR and 200 μM NADH. A final concentration of 1 U mL^{-1} PLE was used for HyCL-4-AM reads. Luminescence emission was measured for 4 h. Rat liver microsome experiments were conducted in a 96-well plate using final concentrations of 200 μg mL^{-1} RLM, 50 μM NADPH, and 20 μM HyCL-3 or HyCL-4-AM in 20 mM PBS (pH 7.4). The plate was then placed into a Cytation 5 BioTek plate reader. The luminescence was recorded using the luminescence detection mode, end point read type, and setting gain to 135 and temperature to 37 °C for 4 h. Control experiments with probe alone were performed in a separate plate to avoid increased background due to light leakage. Reported values are the average of three technical replicates.

Selectivity Studies of HyCL-3 and HyCL-4-AM.

Selectivity for HyCL-3 and HyCL-4-AM was measured by monitoring the time-dependent full-spectrum chemiluminescent emission using a Cytation 5 BioTek plate reader (Winooski, VT) using the luminescence detection method, end point read type, and setting gain to 135 and temperature to 37 °C. All assays were performed in 20 mM PBS buffered to pH 7.4. All analytes were tested with a final concentration of 200 μM for all metal species, 5 mM for GSH, 1 mM for cysteine, and 200 μM for Na_2S. Reported values are the average of three technical replicates from 0 to 50 at 10 min increments. Further details can be found in the Supporting Information.

Cell Culture Conditions and Hypoxia Studies.

Human lung adenocarcinoma epithelial cells (A549) cells were purchased from ATCC and cultured in Ham's F-12K (Kaighn's) medium supplemented with 10% fetal bovine serum (FBS) and 1% antibiotics (penicillin/streptomycin, 100 U/mL). Cells were maintained in a humidified incubator at 37 °C with 5% CO_2. One or 2 days before the experiment, cells were passaged and plated on Costar 12-well plates by adding 150 K–200 K of cells per well, filling each well up to 1 mL of medium. Chemiluminescence responses were measured using a Cytation 5 BioTek plate reader. Before imaging, the medium was removed upon 90%—95% confluency and the cells were washed with 1 mL PBS. Each well was filled with 996

μL F-12K media. Then, 4 μL of 10 mM HyCL-4-AM or HyCL-3 in DMSO (40 μM final concentration) was added to each well and immediately placed into a Cytation 5 BioTek plate reader. The luminescence was recorded using the luminescence detection mode, end point read type. The temperature was set at 37 °C, O_2 level was set to 0.5%–1% or 20%, and CO_2 was set at 5%. Each experiment consisted of three technical replicates for each condition, and each experiment was repeated with three or four biological replicates on separate days. The reported chemiluminescence intensity values are the average of a total of 9–12 wells across three or four biological replicates.

Hypoxia Imaging in Living Mice.

The UT Southwestern Institutional Animal Care and Use Committee approved these investigations under Animal Protocol Number (APN #2017–102329). Tumor xenografts were established by subcutaneous injection of MDA-MB-231 cells into the flanks of athymic nude mice. Mice were placed on a breathing regimen of 16% or 100% O_2 for 10 min, then anesthetized and maintained using inhalation of 2.5% isoflurane, while breathing 16% or 100% O_2. The anesthetized mice were administered intratumoral (IT) or intramuscular (IM) injections of 30 μL, of 120 μM HyCL-4AM (20 mM PBS buffer containing 2.4% DMSO). Images were acquired every 60 s using a Caliper Xenogen IVTS Spectrum (PerkinElmer, Santa Clara, CA) with auto exposure, medium binning, f-stop set to 1, blocked excitation, open emission, FOV set to C, and height set to 1.5. Reported values are the average photon flux from three to six mice.

RESULTS AND DISCUSSION

Design and Synthesis of HyCL-3 and HyCL-4 AM.

In previous work, our lab has shown the efficacy of reaction-based hypoxia probes with HyCL-2.[24] This features a chemiluminescent 1,2-dioxetane scaffold masked by a *para*-nitrobenzyl group through an ether linkage. This *para*-nitrobenzyl group undergoes self-immolative cleavage in response to enzymatic reduction from nitroreductase enzymes. The released phenolate-dioxetane species undergoes decomposition and concomitant luminescence emission via a chemically initiated electron exchange luminescence (CIEEL) mechanism. In continuation of our efforts to develop chemiluminescent probes for tumor hypoxia imaging, we sought methods to increase probe sensitivity for cellular measurements. We took a multifaceted approach to this challenge and designed HyCL-3 and HyCL-4-AM, which we hypothesized would increase sensitivity through increased chemiluminescence quantum yields, as well as using an acetoxymethyl (AM) ester to improve cellular uptake (Scheme l). A control compound HyCL-4-AM-Cont without the nitroaromatic trigger was also designed to control for effects unrelated to nitroaromatic group reduction.

HyCL-3 was prepared by Mitsunobu coupling of acrylonitrile phenol 1 and *para*-nitrobenzyl alcohol, followed by subsequent [2 + 2] cycloaddition with photogenerated singlet oxygen using Rose bengal as a photosensitizer (Scheme 2). Synthesis of HyCL-4-AM began with an S_N2 reaction of phenol 2 and *para*-nitrobenzyl tosylate, followed by hydrolysis of the methyl ester to yield carboxylic acid 3. We then appended the acetoxymethyl ester through an S_N2

reaction with bromomethyl acetate. Finally, we subjected this precursor to a [2 + 2] cycloaddition with singlet oxygen to achieve HyCL-4-AM. The control compound, HyCL-4-AM-Cont was prepared using analogous procedures using benzyl bromide in place of *para*-nitrobenzyl tosylate.

Upon synthesis of HyCL-3 and HyCL-4-AM, their responses toward bacterial nitroreductase and cofactor reduced nicotinamide adenosine dinucleotide (NADH) were examined (Figure 1). Luminescence emission spectra for HyCL-3 and HyCL-4-AM were collected using an F-7000 Hitachi spectrophotometer by treating 10 μM HyCL-3 with 1 μg mL^{-1} nitroreductase (NTR) and 0.2 mM NADH in 20 mM PBS buffer, revealing an emission peak centered at 525 nm (Figure 1A), whereas 10 μM HyCL-4-AM shows an emission maximum at 516 nm when treated with 1 μg mL^{-1} NTR, 0.2 mM NADH, and 1 U mL^{-1} esterase to cleave the AM ester (Figure 1B). The dose dependence of the luminescence emission with regard to nitroreductase was evaluated from 0–1 μg mL^{-1}NTR for HyCL-3 and HyCL-4-AM using a luminescence plate reader (Figure 1C). While HyCL-4-AM showed a clear dose dependence under these conditions, the relative emission intensity for HyCL-3 was much lower and higher enzyme concentrations were required to observe a dose-dependence (Figure S1). The time-course of the chemiluminescence emission of HyCL-4-AM reached a maximum at around 15 min (Figure 1D). The reaction products of HyCL-3 and HyCL-4-AM were analyzed by GC/MS and a peak definitively assigned to 2-adamantanone (*m/z* = 150.1, $M^{+\bullet}$) as well as one tentatively assigned to (4-(hydroxyamino)phenyl)-methanol (*m/z* = 138.8, $M^{+\bullet}$) were found for both probes (Figures S2–S5).

We next studied the in vitro response to rat liver microsomes (RLM), a more relevant model to mammalian hypoxia due to the prevalence of cytochrome P450 reductases in the RLM (Figure 2). Solutions of 20 μM HyCL-3 with 50 μM cofactor reduced nicotinamide adenine dinucleotide phosphate (NADPH) and 200 μg mL^{-1} RLM in 20 mM PBS (pH = 7.41) were incubated for 4 h at 37 °C and compared against solutions of only 20 μM HyCL-3 in 20 mM PBS (pH = 7.4) as a negative control. Under these conditions, HyCL-3 showed a 37-fold increase in peak luminescence at 80 min versus the control, and a glow that persisted for more than 4 h (Figure 2A). By comparison, the same experiment with 20 μM HyCL-4-AM, which showed a more rapid onset of the peak intensity after 20 min, with a phenomenal 60,000-fold increase in luminescence intensity versus the probe alone (Figure 2B).[39] Knowing that HyCL-3 and HyCL-4-AM were sensitive to enzymatic reduction by RLM and NTR, we performed selectivity studies with other biologically relevant reductive species, including metal cations and nucleophilic thiols. The response of 20 μM HyCL-3 or HyCL-4-AM to RLM was monitored against analytes in PBS buffer (20 mM, pH = 7.4) by adding 200 μM CuI, 200 μM $Cu(OTf)_2$, 200 μM $Fe(OTf)_2$, 200 μM $Fe(OTf)_3$, 200 μM $Mn(OTf)_2$, 200 μM $Co(OAc)_2$, 200 μM $Ni(OTf)_2$, 200 μM $Zn(OAc)_2$, 5 mM reduced glutathione (GSH), 1 mM L-cysteine, or 200 μM Na_2S (Figure 2C,D). Both HyCL-3 and HyCL-4-AM showed good selectivity and no significant increase in luminescence intensity toward any of the selected species over the blank control.

Given that HyCL-4-AM exhibited higher sensitivity than HyCL-3, we decided to proceed with HyCL-4-AM as our primary agent for hypoxia detection in cellular models (see Figure S6 for HyCL-3 cellular data). We first tested the cellular toxicity of HyCL-4-AM using an

MTT assay, which showed no significant reduction to cell growth at the tested concentrations (Figure S7). Next we tested whether HyCL-4-AM could distinguish hypoxic and normoxic conditions in A549 cells. Cells in 12-well plates were treated with 40 μM HyCL-4-AM or 40 μM HyCL-4-AM and 500 μM diphenyleneiodonium chloride (DPI, a broad spectrum inhibitor of cytochrome P450 reductase)[40] and directly placed into a luminescence plate reader at 37 °C with 5% CO_2 and either 1% or 20% O_2 conditions for 20 h. In all conditions, HyCL-4-AM showed an emission maximum after approximately 1 h (Figure 3A,B). Interestingly, HyCL-4-AM exhibited a sharp decline from intensity maximum over 7 h to near baseline values when incubated at 1% O_2(Figure 3A), whereas a slower decrease in chemiluminescence intensity over 19 h was observed in cells that were monitored under a 20% O_2 atmosphere (Figure 3B). Comparison to the cellular response of the carboxylate HyCL-4 demonstrated the dramatic effect of the acetoxymethyl ester for efficient cellular operation (Figure S8). While HyCL-4-AM showed a clear response over 4 h in the presence of A549 cells, with no response from cell culture media in the absence of cells (Figure S8A), HyCL-4 showed only a very bright background that rapidly decays with no clear difference in the presence or absence of cells (Figure S8B). Furthermore, treatment with 500 μM DPI at 1% O_2 slows the decay and yields a result indistinguishable from the response at 20% O_2 (Figure 3A,B), demonstrating that DPI has an effect similar to that of O_2. Comparison of the cellular response of HyCL-4-AM at 1% versus 20% O_2 showed a highly significant and reproducible *reduction* in luminescence emission under hypoxic conditions (Figure 3C,D).

This, at first, appears contradictory to established literature on biological nitroaromatic reduction chemistry, but can be understood when considering the kinetics of chemiluminescence emission. The rate of chemiluminescence decomposition of the acrylic acid dioxetane phenol released by HyCL-4-AM was measured to be 5.47×10^{-3} s^{-1} and completely decayed within 15 min at pH 7.4 (Figure S9A), approximately ten times more rapidly than the acrylonitrile dioxetane phenol (Figure S9B). In cells, it takes more than 150 min for the signal decay, indicating that nitroaromatic group reduction is the rate-limiting step for producing chemiluminescence. We modeled the cellular chemiluminescence response as an X to Y to Z consecutive reaction (Figure S10), where the first rate constant k_1 accounts for cell uptake and ester cleavage and the second rate constant k_2 accounts for the rate of chemiluminescence emission, which is limited by the rate of nitroaromatic reduction. This is modeled by the rate eq 1, where y is the relative emission intensity, k_1 is the rate of cell uptake and ester cleavage, k_2 is the rate of nitroaromatic group reduction, A is a parameter proportional to the initial concentration of the probe, and B is a parameter to fit the background:

$$y = A\frac{k_1}{k_2 - k_1}\left(e^{-k_1 t} e^{-k_2 t}\right) + B \quad (1)$$

Fitting the cellular data to this model (Figure S10C,D) shows that the rate constant k_1 does not significantly change but k_2 significantly decreases from 2.82×10^{-4} M^{-1} s^{-1} at 1% O_2 to 1.79×10^{-5} M^{-1} s^{-1} at 20% O_2 (Figure 3E), consistent with O_2 inhibition of nitroreductase

activity. This model demonstrates that HyCL-4-AM can provide a numerical measure of the inhibition of endogenous nitroreductase activity by O_2. By comparison, 40 μM HyCL-4-AM-Cont in A549 cells showed only baseline luminescence emission over the same conditions and time span (Figure 3F), confirming the requirement of nitroreductase activity for the chemiluminescence response.

After demonstrating that HyCL-4-AM displayed an alteration in chemiluminescence kinetics dependent on O_2 levels, we sought to investigate its behavior in animal models. We subcutaneously implanted the flanks of athymic nude mice with MDA-MB-231 breast cancer cells and allowed the tumors to grow to appropriate size for hypoxia testing. The mice were set to breathe 16% O_2 with 2.5% isoflurane for 10 min and then treated with 30 μL, of 120 μM HyCL-4-AM via intratumoral (IT) injection. These were compared with mice administered with the same amount of HyCL-4-AM via intramuscular (IM) injection. Images were acquired every minute for 100 min using an IVIS Spectrum. HyCL-4-AM showed a strong output signal with kinetics dictated by the degree of oxygenation of the tissue (Figure 4). By comparing the response of chemiluminescence emission over 100 min, the decay in signal in the hypoxic tumor tissue at 16% O_2 was faster than in the well oxygenated muscle tissue (Figure 4A), consistent with the results of our cellular studies.

Hyperoxic treatments have been explored as a theranostic method to characterize, oxygenate, and sensitize tumors.[11,41] When mice were set to breath 100% O_2, the response of HyCL-4-AM returned to the values of the IM injection, showing that hyperoxic treatment can reoxygenate tumors and this tumor response can be monitored using HyCL-4-AM (Figure 4B). Comparison between IT injections with mice breathing 16% O_2 versus 100% O_2 showed that, on average, signal decayed more rapidly when mice breathe 16% O_2 (Figure 4C). It was observed, however, that different tumors responded differently to hyperoxic treatment, indicating potential for HyCL-4-AM to differentiate between tumors that respond to hyperoxic treatment from those that do not. Representative images from mice 60 min after injection showed differentiation between hypoxic and well oxygenated tissues (Figure 4D–F). Overall, these results show that HyCL-4-AM can effectively distinguish hypoxic tumors from healthy tissue in vivo.

CONCLUSIONS

In conclusion, we have synthesized HyCL-3 and HyCL-4-AM as chemiluminescent indicators of hypoxia in cellular and animal models. Both probes are selective for enzymatic reduction of the nitroaromatic group as exhibited through reaction with bacterial nitroreductase and NADH as well as rat liver microsomes in conjunction with NADPH. Due to increased sensitivity, HyCL-4-AM was further tested in cells, where it exhibited a highly significant difference in chemiluminescence emission when cells were subjected to hypoxic conditions as compared to normoxic conditions. Furthermore, robust animal studies demonstrated the ability of HyCL-4-AM to measure and image hypoxia in tumor xenograft models. The observed inhibition of reductase activity in oxygenated tissue is consistent with the response expected from one-electron mammalian reductase enzymes and is unlikely to be due to oxygen-independent bacterial nitroreductase activity. In comparison to the recently published CL-NTR,[25] the inclusion of the AM ester moiety provides a drastic increase in

sensitivity and response due to increased cell uptake. This opens up the possibility of high throughput cell experiments that have thus far not been reported for previous chemiluminescent probes HyCL-2[24] and CL-NTR.[25] HyCL-4-AM provides a maximum photon flux of more than 1×10^7 photons s^{-1} in tumor xenografts, which is ca. 1000-fold greater than previously reported chemiluminescent hypoxia probes.[24,25] This kinetics-based approach to monitoring cellular hypoxia is a significant advance in chemiluminescence detection technology since the reaction kinetics are less dependent on tumor size and depth of injection, which can vary greatly between experiments and could explain potential differences in results from less sensitive probes. This study establishes that HyCL-4-AM is a highly reproducible tool to investigate hypoxia in cells and has efficacy in monitoring tumor oxygenation in animal models. More generally, we showed that installation of an AM ester provides a versatile strategy for using 1,2-dioxetane probes in cellular systems.

Supplementary Material

Refer to Web version on PubMed Central for supplementary material.

ACKNOWLEDGMENTS

This work was supported by the National Institutes of Health (NIH) under R15GM114792, the National Science Foundation under CHE 1653474, and optical imaging was performed using an IVIS purchased under NIH 1S10RR024757 and supported by NIH P30 CA142543. We acknowledge Daphne Nguyen and Alexander Winters for experimental assistance and thank Maciej Kukula (UT Arlington) for assistance with mass spectrometry.

REFERENCES

(1). Aragonés J; Fraisl P; Baes M; Carmeliet P Oxygen sensors at the crossroad of metabolism. Cell Metab 2009, 9, 11–22. [PubMed: 19117543]

(2). Krock BL; Skuli N; Simon MC Hypoxia-induced angiogenesis: good and evil. Genes Cancer 2011, 2, 1117–1133. [PubMed: 22866203]

(3). Pennacchietti S; Michieli P; Galluzzo M; Mazzone M; Giordano S; Comoglio PM Hypoxia promotes invasive growth by transcriptional activation of the met protooncogene. Cancer Cell 2003, 3, 347–361. [PubMed: 12726861]

(4). Sullivan R; Graham CH Hypoxia-driven selection of the metastatic phenotype. Cancer Metastasis Rev 2007, 26, 319–331. [PubMed: 17458507]

(5). Sendoel A; Hengartner MO Apoptotic cell death under hypoxia. Physiology 2014, 29, 168–176. [PubMed: 24789981]

(6). Schnitzer SE; Schmid T; Zhou J; Brüne B Hypoxia and HIF-1alpha protect A549 cells from drug-induced hypoxia. Cell Death Differ 2006, 13, 1611–1613. [PubMed: 16456580]

(7). Le QT; Chen E; Salim A; Kong CS; Whyte R; Donington J; Cannon W; Wakelee H; Tibshirani R; Mitchell JD; Richardson D; O'Byrne KJ; Koong AC; Giaccia AJ An evaluation of tumor oxygenation and gene expression in patients with early stage non-small cell lung cancers. Clin. Cancer Res 2006, 12, 1507–1514. [PubMed: 16533775]

(8). Dehdashti F; Grigsby PW; Mintun MA; Lewis JS; Siegel BA; Welch MJ Assessing tumor hypoxia in cervical cancer by positron emission tomography with 60Cu-ATSM: relationship to therapeutic response-a preliminary report. Int. J. Radiat. Oncol., Biol., Phys 2003, 55, 1233–1238. [PubMed: 12654432]

(9). Tatum JL; Kelloff GJ; Gillies RJ; Arbeit JM; Brown JM; Chao KS; Chapman JD; Eckelman WC; Fyles AW; Giaccia AJ; Hill RP; Koch CJ; Krishna MC; Krohn KA; Lewis JS; Mason RP; Melillo G; Padhani AR; Powis G; Rajendran JG; Reba R; Robinson SP; Semenza GL; Swartz HM; Vaupel P; Yang D; Croft B; Hoffman J; Liu GY; Stone H; Sullivan D Hypoxia: importance in

tumor biology, noninvasive measurement by imaging, and value of its measurement in the management of cancer therapy. Int. J. Radiat. Biol 2006, 82, 699–757. [PubMed: 17118889]

(10). Taylor NJ; Baddeley H; Goodchild KA; Powell ME; Thoumine M; Culver LA; Stirling JJ; Saunders MI; Hoskin PJ; Phillips H; Padhani AR; Griffiths JR BOLD MRI of tumor oxygenation during carbogen breathing. J. Magn. Reason. Imaging 2001, 14, 156–163.

(11). Zhou H; Hallac RR; Yuan Q; Ding Y; Zhang Z; Xie XJ; Francis F; Roehrborn CG; Sims RD; Costa DN; Raj GV; Mason RP Incorporating oxygen-enhanced MRI into multi-parametric assessment of human prostate cancer. Diagnostics 2017, 7, E48. [PubMed: 28837092]

(12). Liu JN; Bu W; Shi J Chemical design and synthesis of functionalized probes for imaging and treating tumor hypoxia. Chem. Rev 2017, 117, 6160–6224. [PubMed: 28426202]

(13). Krohn KA; Link JM; Mason RP Molecular imaging of hypoxia. J. Nucl. Med 2008, 49, 129S–148S. [PubMed: 18523070]

(14). Wang CY; Behrens BC; Ichikawa M; Bryan GT Nitroreduction of 5-nitrofuran derivatives by rat liver xanthine oxidase and reduced nicotinamide adenine dinucleotide phosphate-cyto-chrome c reductase. Biochem. Pharmacol 1974, 23, 3395–3404. [PubMed: 4155308]

(15). Wardman P; Clarke ED Oxygen inhibition of nitroreductase: electron transfer from nitro radical-anions to oxygen. Biochem. Biophys. Res. Commun 1976, 69, 942–949. [PubMed: 6027]

(16). Peterson FJ; Mason RP; Hovsepian J; Holtzman JL Oxygen-sensitive and -insensitive by Escherichia coli and rat hepatic microsomes. J. Biol. Chem 1979, 254, 4009–4014. [PubMed: 374406]

(17). Leskovac V; Popovic M Mechanism of reduction of nitrofurantoin on liver microsomes. Pharmacol. Res. Commun 1980, 12, 13–27. [PubMed: 7384160]

(18). Raleigh JA; Shum FY; Koziol DR; Saunders WM Structure-function dependence and allopurinol inhibition of radiosensitizer/nitroreductase interaction: approaches to improving therapeutic ratios. Cancer Clin. Trials 1980, 3, 55–62. [PubMed: 6771029]

(19). Clarke ED; Goulding KH; Wardman P Nitroimidazoles as anaerobic electron acceptors for xanthine oxidase. Biochem. Pharmacol 1982, 31, 3237–3242. [PubMed: 6897358]

(20). Tsai CS Nitroreductase activity of heart lipoamide dehydrogenase. Biochem. J 1987, 242, 447–452. [PubMed: 3593260]

(21). Wilson WR; Hay MP Targeting hypoxia in cancer therapy. Nat. Rev. Cancer 2011, 11, 393–410. [PubMed: 21606941]

(22). Knox HJ; Hedhli J; Kim TW; Khalili K; Dobrucki LW; Chan J A bioreducible N-oxide-based probe for photoacoustic imaging of hypoxia. Nat. Commun 2017, 8, 1794. [PubMed: 29176550]

(23). Gao Y; Lin Y; Liu T; Chen H; Yang X; Tian C; Du L; Li M Bioluminescent probe for tumor hypoxia detection via CYP450 reductase in living animals. Anal. Chem 2017, 89, 12488–12493. [PubMed: 29073759]

(24). Cao J; Campbell J; Liu L; Mason RP; Lippert AR In vivo chemiluminescent imaging agents for nitroreductase and tissue ocygenation. Anal. Chem 2016, 88, 4995–5002. [PubMed: 27054463]

(25). Sun J; Hu Z; Wang R; Zhang S; Zhang X A highly sensitive chemiluminescent probe for detecting nitroreductase and imaging in living animals. Anal. Chem 2019, 91, 1384–1390. [PubMed: 30582678]

(26). Vacher M; Fdez Galván I; Ding BW; Schramm S; Berraud-Pache R; Naumov P; Ferré N; Liu YJ; Navizet I; Roca-Sanjuán D; Baader WJ; Lindh R Chem and bioluminescence of cyclic peroxides. Chem. Rev 2018, 118, 6927–6974. [PubMed: 29493234]

(27). Gnaim S; Green O; Shabat D The emergence of aqueous chemiluminescence: a promising class of 1,2-dioxetane lumiphores. Chem. Commun 2018, 54, 2073–2085.

(28). Ryan LS; Lippert AR Ultrasensitive chemiluminescent detection of cathepsin B: insights into the new frontier of chemiluminescet imaging. Angew. Chem., Int. Ed 2018, 57, 622–624.

(29). Green O; Eilon T; Hananya N; Gutkin S; Bauer CR; Shabat D Opening a gateway for chemiluminescence cell imaging: distinctive methodology for design of bright chemiluminescent dioxetane probes. ACS Cent. Sci 2017, 3, 349–358. [PubMed: 28470053]

(30). Lippert AR Unlocking the potential of chemiluminescence imaging. ACS *Cent. Sci.* 2017, 3, 269–271. [PubMed: 28470041]

(31). Hananya N; Reid JP; Green O; Sigman MS; Shabat D Rapid chemiexcitation of phenoxy-dioxetane luminophores yields ultrasensitive chemiluminescence assays. Chem. Sci 2019, 10, 1380–1385. [PubMed: 30809354]

(32). Cao J; An W; Reeves AG; Lippert AR A chemiluminescent probe for cellular peroxynitrite using a self-immolative oxidative decarbonylation reaction. Chem. Sci 2018, 9, 2552–2558. [PubMed: 29732134]

(33). An W; Ryan LS; Reeves AG; Bruemmer KJ; Mouhaffel M; Gerberich JL; Winters A; Mason RP; Lippert AR A chemiluminescent probe for HNO quantification and real-time monitoring in living cells. Angew. Chem., Int. Ed 2019, 58, 1361–1365.

(34). Bruemmer KV; Green O; Su TA; Shabat D; Chang CJ Chemiluminescent probes for activity-based sensing of formaldehyde from folate degradation in mice. Angew. Chem., Int. Ed 2018, 57, 7508–7512.

(35). Gnaim S; Scomparin A; Das S; Blau R; Satchi-Fainaro R; Shabat D Direct real-time monitorig of prodrug activation by chemiluminescence. Angew. Chem., Int. Ed 2018, 57, 9033–9037.

(36). Roth-Konforti M; Bauer CR; Shabat D Angew. Chem., Int. Ed 2017, 56, 15633–15638.

(37). Son S; Won M; Green O; Hananya N; Sharma A; Jeon Y; Kwak JH; Sessler JL; Shabat D; Kim JS Chemiluminescent probe for the in vitro and in vivo imaging of cancrs over-expressing NQO-1. Angew. Chem., Int. Ed 2019, 58, 1739–1743.

(38). Gao Y; Lin Y; Liu T; Zhang X; Xu F; Liu P; Du L; Li M A specific and selective chemiluminescent probe for Pd2+ detection. Chin. Chem. Lett 2019, 30, 63–66.

(39). We note that these high turn-on values are achieved using freshly purified HyCL-4-AM and performing the control in a separate plate to avoid light leakage from adjacent wells. Light leakage from experiments in adjacent wells and impurities can increase the background signal by ca. 100-fold.

(40). Tew DG Inhibition of cytochrome P450 reductase by the diphenyliodonium cation. Kinetic analysis and covalent modifications. Biochemistry 1993, 32, 10209–10215. [PubMed: 8399148]

(41). Zhou H; Belzile O; Zhang Z; Wagner J; Ahn C; Richardson JA; Saha D; Brekken RA; Mason RP The effect of flow on blood oxygen level dependent (R^*_2) MRI of orthotopic lung tumors. Magn. Reson. Med 2019, 81, 3787–3797. [PubMed: 30697815]

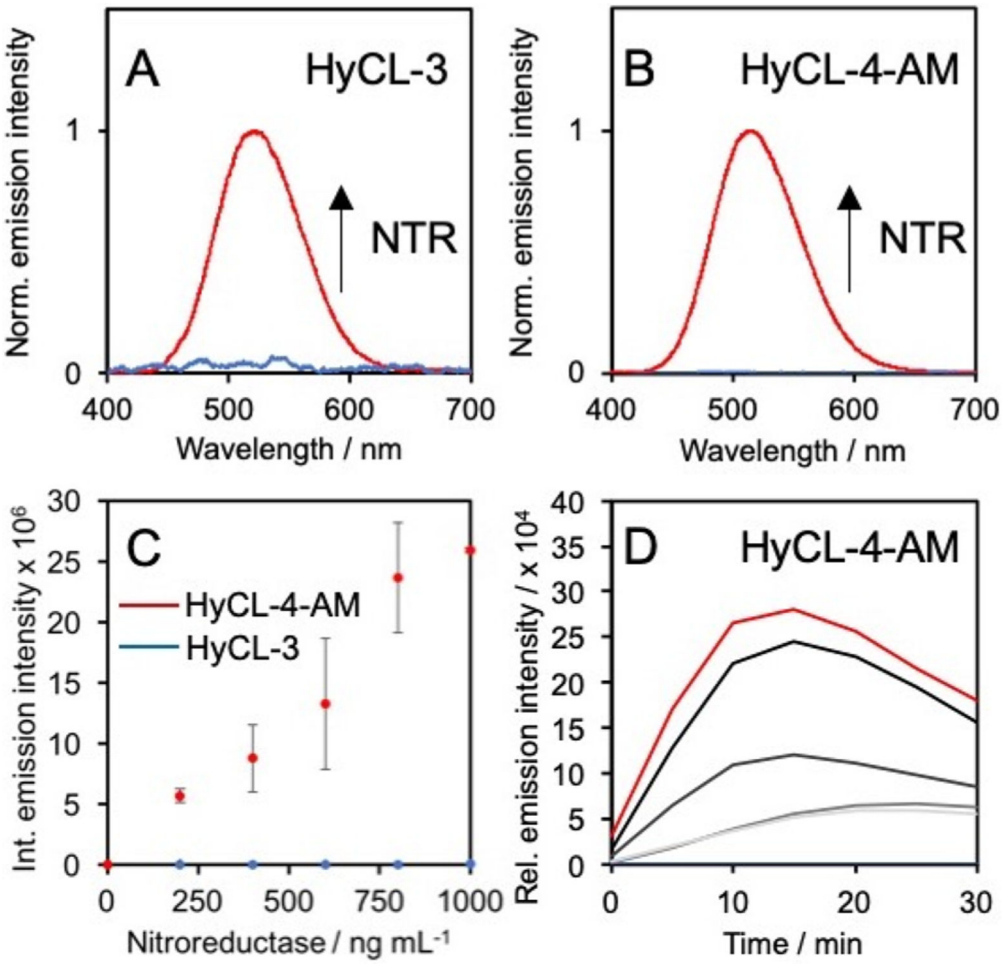

Figure 1.

Response of HyCL-3 and HyCL-4-AM. Chemiluminescence emission spectra of (A) 10 μM HyCL-3 (blue trace) before and (red trace) after treatment with 1 μg mL^{-1} NTR and 0.2 mM NADH and (D) 10 μM HyCL-4-AM (blue trace) before and (red trace) after treatment with 1 μg mL^{-1} NTR, 0.2 mM NADH, and 1 U mL^{-1}PLE. (C) Integrated emission intensity of 10 μM HyCL-4-AM (red trace) or HyCL-3 (blue trace) alone or with 200–1000 ng mL^{-1} NTR and 0.2 mM NADH. PLE (1 U mL^{-1}) was added for HyCL-4-AM. (D) Time-course of the chemiluminescence emission of 10 μM HyCL-4-AM alone (blue trace) or with 200, 400, 600, 800, and (red trace) 1000 ng mL^{-1} NTR, 0.2 mM NADH, and 1 U mL^{-1} PLE. All experiments were performed in 20 mM PBS (pH 7.4) containing ≤1% DMSO. Error bars are ± SD.

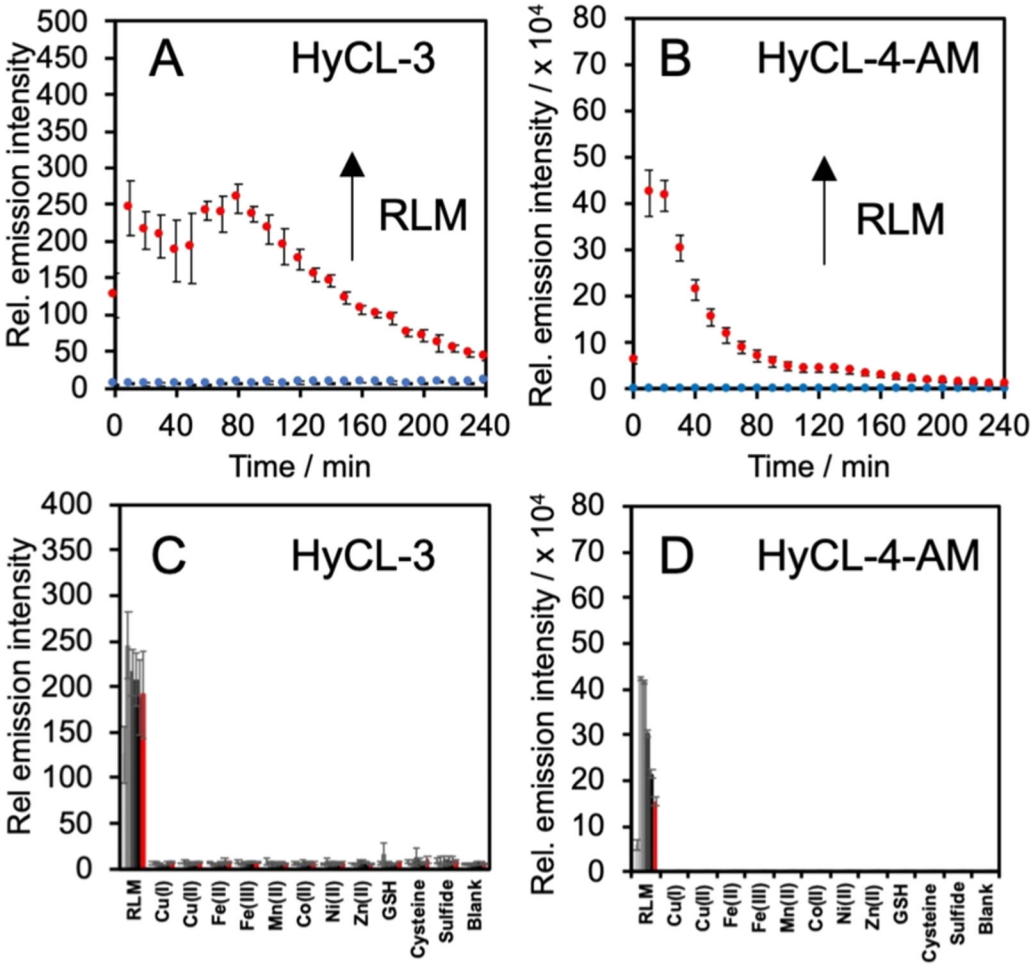

Figure 2.

Selectivity of HyCL-3 ad HyCL-4-AM. Response of (A) 20 μM HyCL-3 in the (blue trace) absence and (red trace) presence of 200 μg mL^{-1} rat liver microsomes (RLM) and 50 μM NADPH and (B) 20 μM HyCL-4-AM in the (blue trace) absence and (red trace) presence of 200 μg mL^{-1} rat liver microsomes (RLM) and 50 μM NADPH. Response of (C) 20 μM HyCL-3 and (D) 20 μM HyCL-4-AM to the indicated analytes from 0 to (red bars) 50 at 10 min increments. All experiments were performed in 10 mM PBS (pH 7.4) containing ≤1% DMSO. Error bars are ± SD.

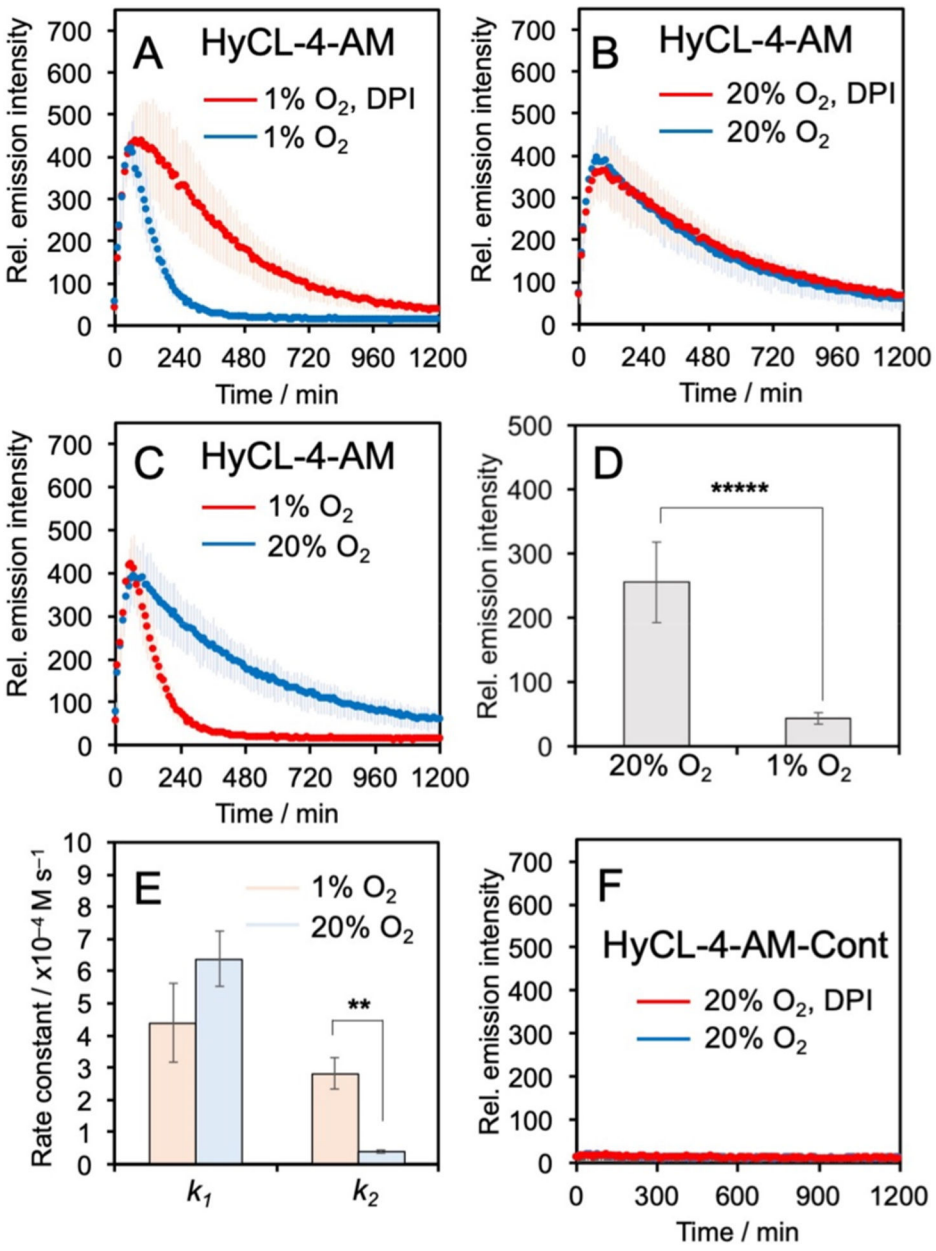

Figure 3.

Measuring hypoxia in living A549 cells. (A–C) Time-course of the chemiluminescence emission of A549 cells incubated with 40 μM HyCL-4-AM at 1% O_2 or 20% O_2 in the presence or absence of DPI. (D) Chemiluminescence emission intensity at 300 min of A549 cells incubated with 40 μM HyCL-4-AM at 1% O_2 or 20% O_2. (E) Measured rate constants for the cellular response of HyCL-4-AM. (F) Time-course of the chemiluminescence emission of A549 cells incubated with 40 μM HyCL-4-AM-Cont at 20% O_2 in the presence or absence of DPI. All experiments were performed in F12K containing 10% FBS and ≤1% DMSO. Error bars are ± SD. Statistical significance was assessed using a two-tailed Student's *t* test. $^{**}p < 0.005$ (n = 3–4 biological replicates), $^{***}p < 5 \times 10^{-6}$ (n =9–12 wells across 3–4 biological replicates).

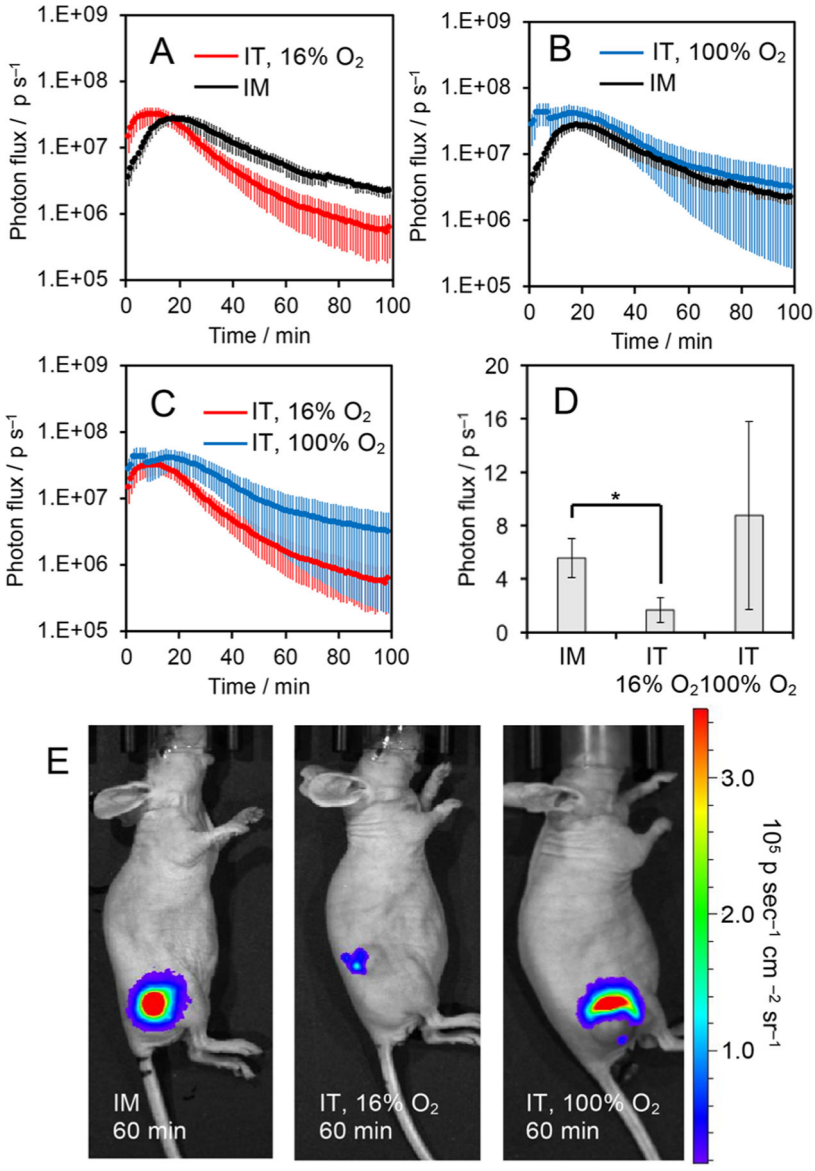

Figure 4.

Measuring oxygenation in healthy muscle tissue and tumor xenografts. (A–C) Time course of the chemiluminescence emission of 30 of 120 μM HyCL-4-AM in 20 mM PBS (pH 7.4) containing 2.4% DMSO in athymic nude mice after intramuscular (IM) injection into the flank, intratumoral injection while mice were breathing 16% O_2 (IT, 16% O_2), and intratumoral injection while mice were breathing 100% O_2 (IT, 100%). (D) Photon flux and (E) chemiluminescence images of athymic nude mice 60 min after IM injection, IT injection while mouse breathed 16% O_2, and after IT injection while mouse breathed 100% O_2. Error bars are ± SE from n = 3–6 mice. Statistical significance was assessed using a two-tailed Student's t test. $^*p < 0.05$.

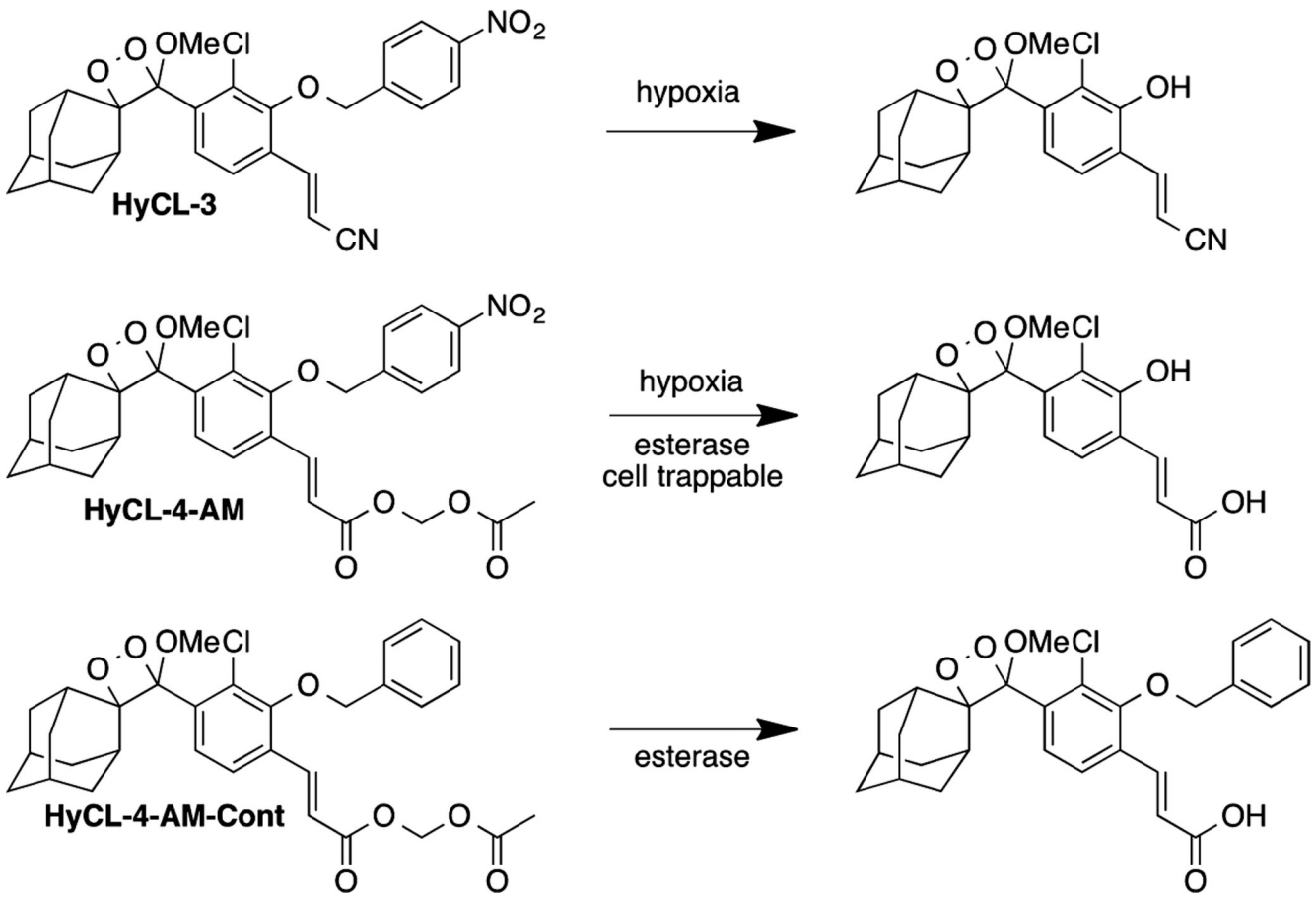

Scheme 1.
Probe Designs and Sensing Reactions for HyCL-3, HyCL-4-AM, and HyCL-4-AM-Cont).

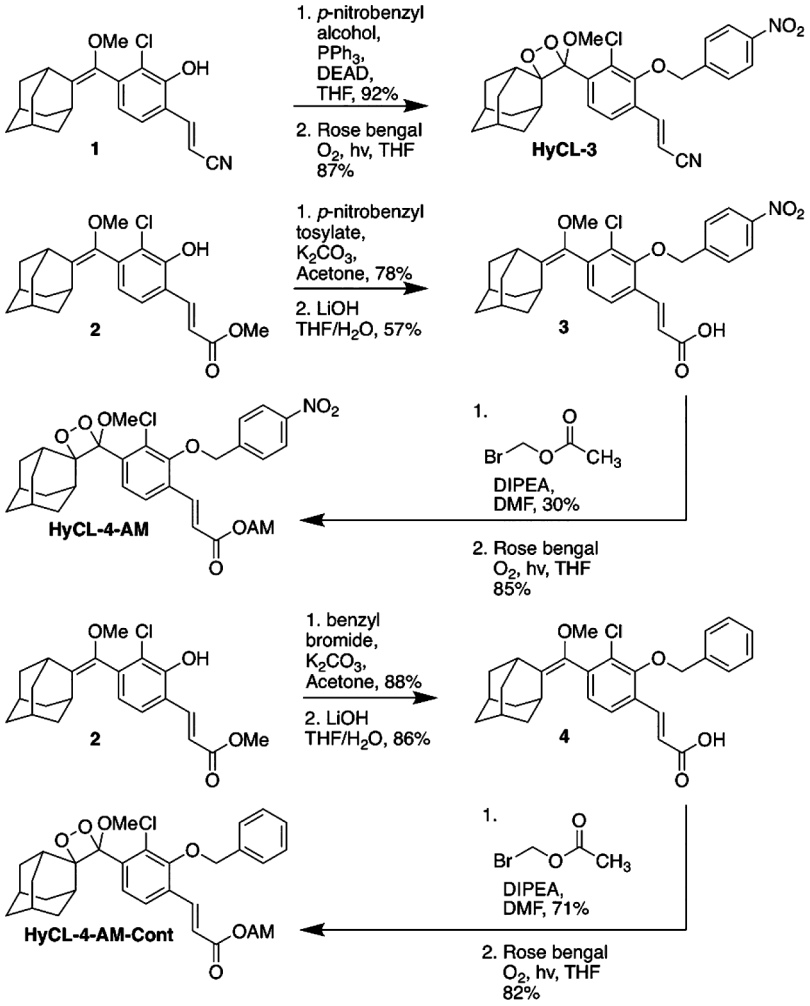

Scheme 2.
Synthesis of HyCL-3, HyCL-4-AM, and HyCL-4-AM-Cont